1   Supporting Information for:

2   Incorporation of uranium into hematite during crystallization from

3   ferrihydrite.

4   *Timothy A. Marshall,[†] Katherine Morris,[†] Gareth T.W. Law,[‡] Francis R. Livens,[‡], J. Frederick W.*

5   *Mosselmans,[§] Pieter Bots,[†] and Samuel Shaw [†][*]*

6   † Research Centre for Radwaste and Decommissioning and Williamson Research Centre for Molecular

7   Environmental Science, School of Earth, Atmospheric and Environmental Sciences, The University of

8   Manchester, Manchester, M13 9PL, UK.

9   ‡ Centre for Radiochemistry Research and Research Centre for Radwaste and Decommissioning, School of

10   Chemistry, The University of Manchester, Manchester, M13 9PL, UK.

11   § Diamond Light Source Ltd, Diamond House, Harwell Science and Innovation Campus, Didcot, Oxfordshire,

12   OX11 0DE, UK.

13   * email: sam.shaw@manchester.ac.uk

14

15   Submitted to ES&T

16

17   Number of pages: 24;

18   Number of Figures: 9 (Figure SI-1 to SI-9);

19   Number of Tables: 8 (Table SI-1 to SI-8);

20

Materials and Methods

All reagents used were of analytical grade and 18.2 MΩ deionized water (DIW) was used throughout. Two-line ferrihydrite was synthesized as per Cornell and Schwertmann.[1] In brief, 1M KOH was added to 0.2 M $Fe(NO_3)_3 \cdot 9H_2O$ whilst stirring to bring the pH to ~7. The suspension was centrifuged and the supernatant discarded. The solids were washed three times in DIW and stored at 5 °C for no more than a week before use. The Fe(III) content of each batch of ferrihydrite slurry was determined using the ferrozine assay[2] after digestion in 4 M HCl. A synthetic cement leachate (pH 10.5) was used to represent groundwater conditions during evolution of the chemically disturbed zone (CDZ) around a cementitious repository.[3] The leachate was prepared by adding 0.015 g L^{-1} analytical grade calcium hydroxide $(Ca(OH)_2)$ to DIW whilst stirring and sparging with zero grade N_2. The solutions were stored in an anaerobic chamber (~ 5 % H_2, balance N_2) maintained at < 1 ppm O_2 and CO_2 throughout sample manipulations.

Ferrihydrite was equilibrated with the cement leachate at a solid/solution ratio of 0.4 gL^{-1} for 1 hour on an orbital shaker at room temperature, and the pH manually adjusted to 10.5 by addition of KOH. The headspace of each experiment was flushed with CO_2-free air to avoid complexation of U(VI) with dissolved CO_3^{2-}. Experiments were spiked with U(VI) to give an initial $U_{(aq)}$ concentration of 1 ppm (4.2 $x10^{-6}$ mol L^{-1}), which was thermodynamically modeled (PHREEQC) to be below the solubility of any U(VI) phase in the synthetic leachate, and left to equilibrate for 24 hours. After this equilibration, the 0 hours sample was taken, and the remaining experiments placed into an oven at 60°C for up to 70 days to induce crystallization to hematite. Parallel experiments were also set up without U(VI) present for BET surface area and XRD analysis. The experiments were agitated daily with pH regularly monitored and adjusted as necessary to maintain the starting pH (± 0.2). Samples were removed from each experiment under flowing CO_2-free air. Solid samples were obtained by centrifugation (4000 rpm, 5 minutes) of the

1   suspension and removal of the supernatant. The resulting wet paste was treated in one of two ways:

2   samples for XRD, BET and TEM were washed three times in DIW to remove any surface salt and stored

3   in a desiccator under CO_2-free conditions; samples for XAS were immediately frozen at -80°C without

4   washing so as not to risk leaching any adsorbed U.

5   For U analysis, aqueous samples were 0.45 µm filtered (nylon membrane), preserved in 4M HNO_3,

6   and analyzed for [238]U by ICP-MS on an Agilent 7500cx. Combined errors have been calculated for each

7   data series. Solids were characterized by XRD using Bruker D8 (λ = Cu K-α_1) and Phillips PW1050 (λ

8   = Cu Kα) diffractometers. Topas 4-2[4] was used for quantitative analysis of the XRD patterns. Surface

9   area was measured using the BET method on a Micromeritics Gemini V analyzer. Particle morphologies

10   were characterized via TEM using an FEI Tecnai TF20 TEM and a Phillips CM200 TEM.

11

TEM Imaging
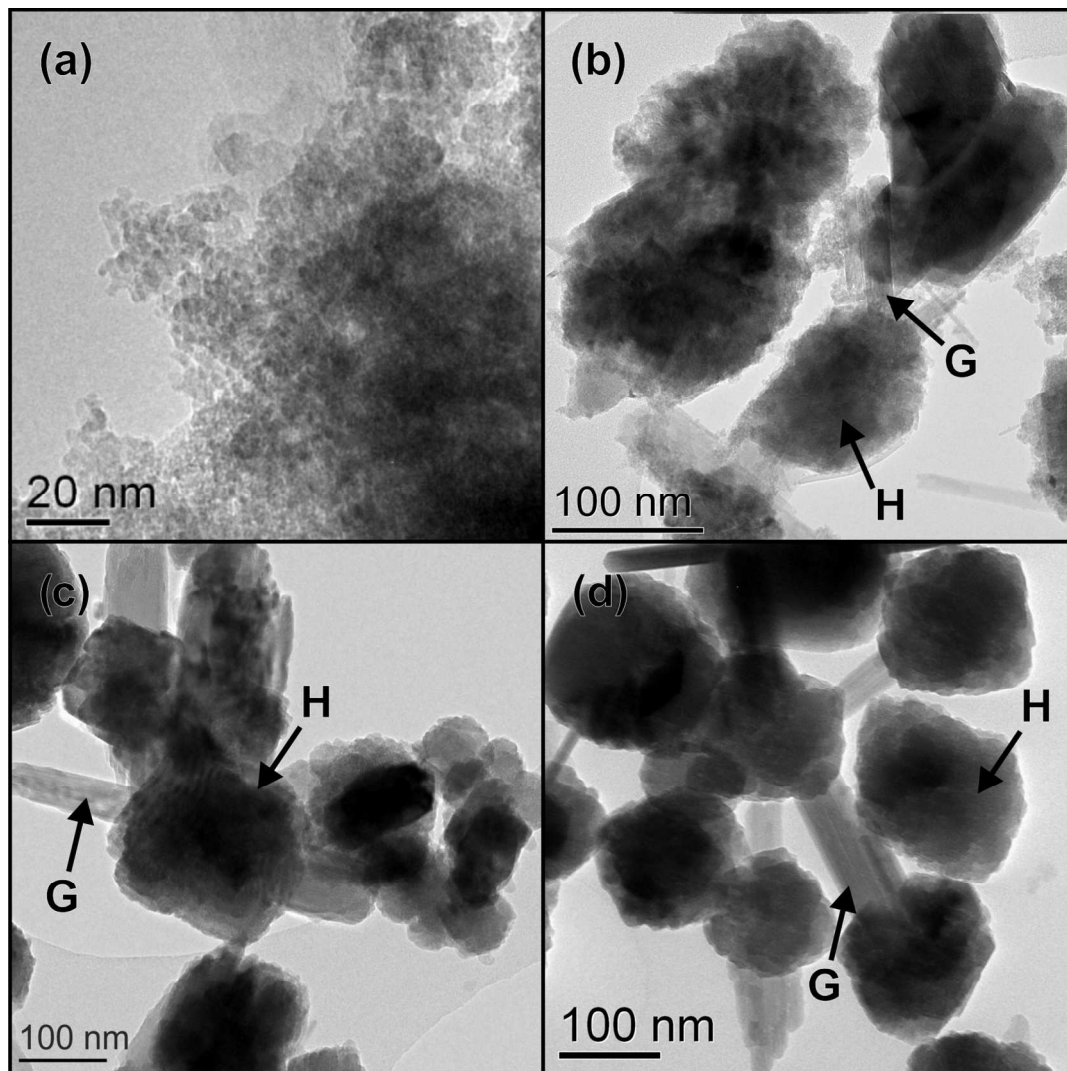
Figure SI- 1 TEM images of hematite/goethite crystallization at 60°C. (a) 0 hours; (b) 24 hours; (c) 7 days; (d) 30 days. H and G indicate hematite and goethite respectively.

1 **Quantitative analysis of XRD patterns**

2   To quantify the proportions of goethite and hematite in the solid samples, Rietveld refinements were

3 performed using Topas 4-2.[4] Topas 4-2 uses the integrated intensity of the diffraction peaks and the

4 crystal structure to calculate the relative mass of each of the phases identified in a solid sample.[5,6]

5 However, distinct Bragg peaks in diffraction patterns were absent for ferrihydrite, due to the

6 nanocrystalline nature of this phase. Two very broad peaks were visible in the diffraction patterns when

7 ferrihydrite was present. The amount of ferrihydrite was calculated using the structure for ferrihydrite

8 derived by Michel et al.[7] with fixed unit cell parameters, and assuming the particle size was constant

9 throughout the experiments. A particle size of approximately 2.5 nm was determined which corresponds

10 well with the collected TEM images.

11

12 Table SI- 1 Quantitative refinement of XRD patterns

Time point		Hematite			Goethite			Ferrihydrite			Total
		wt%		error (wt%)	wt%		error (wt%)	wt%		error (wt%)	wt%
60°C	0H							100.0	±	0.0	100.0
	4H	2.5	±	0.3	3.2	±	0.4	94.3	±	0.6	100.0
	8H	16.1	±	0.7	5.5	±	0.4	78.4	±	0.9	100.0
	12H	32.8	±	0.7	9.6	±	0.3	57.6	±	0.8	100.0
	1D	82.1	±	0.5	17.9	±	0.3				100.0
	2D	74.2	±	0.5	25.8	±	0.5				100.0
	4D	72.0	±	0.6	28.0	±	0.6				100.0
	1W	70.6	±	0.4	29.4	±	0.3				100.0
	2W	63.5	±	0.7	36.5	±	0.7				100.0
	4W	55.3	±	1.6	44.7	±	1.6				100.0
105°C	2W	90.0	±	1.0	10.0	±	0.6				100.0
	6W	90.8	±	0.8	9.2	±	0.8				100.0

13   Blank cell indicates structure not included in refinement

1

2

1 EXAFS Fitting
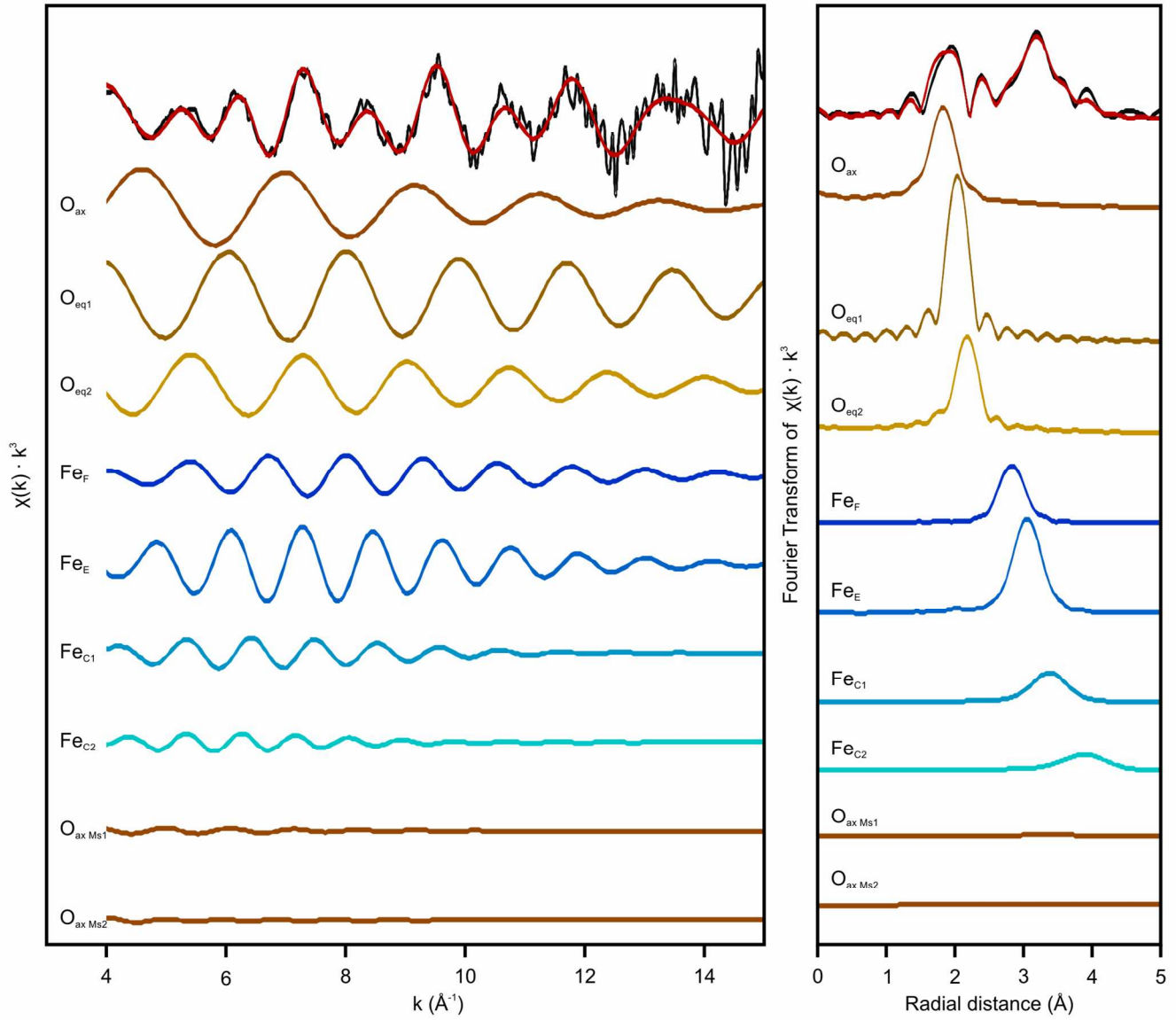
Figure SI- 2 Uranium L_{III}-edge k^3 EXAFS spectra and corresponding Fourier transform of the 105°C data (black line) and model fit of U(VI) incorporation into hematite via substitution for Fe(III) (red line), with theoretical spectral contributions from each modeled path as calculated by Feff6.0.[8] The Fourier Transform is plotted with a phase correction calculated from O_{ax}.

1 **EXAFS Fitting – 105 °C data; O shell fitting**

2   The results of iterative fits to the 105°C data are presented below. The coordination of the shells is

3 shown in Table SI- 2 and the fit plots are shown in Figure SI- 3. Details of the fit parameters are given in

4 Table SI- 5.

5

6 Table SI- 2 Coordination numbers for Fe/O shells within the fitting models applied to the 105°C data.

Fit	(a)	(b)	(c)	(d)	(e)	(f)
O_{ax}		2	2	2	2	2
O_{eq1}	6		2		3	2
O_{eq2}		4	2	2	3	2
Fe_F	1	1	1	1	1	
Fe_E	3	3	3	3	3	
Fe_{C2}	3	3	3	3	3	
Fe_{C2}	6	6	6	6	6	
$O_{ax\ MS}$*		2	2	2	2	2

7   Blank cell indicates shell was omitted from the fitting model

8

Figure SI- 3 EXAFS fits (red) to 105°C data (black). Details of fit and fit parameters are given in Table SI- 5. The Fourier Transforms are plotted with a phase correction calculated from O_{ax} in each case.

1 **EXAFS Fitting – 105 °C data; effect of additional Fe shells and uncoordinated Fe shells**

2   The results of iterative fits to the 105°C data are presented below. The coordination of the shells is

3 shown in Table SI- 3 and the fit plots are shown in Figure SI- 4. Details of the fit parameters are given in
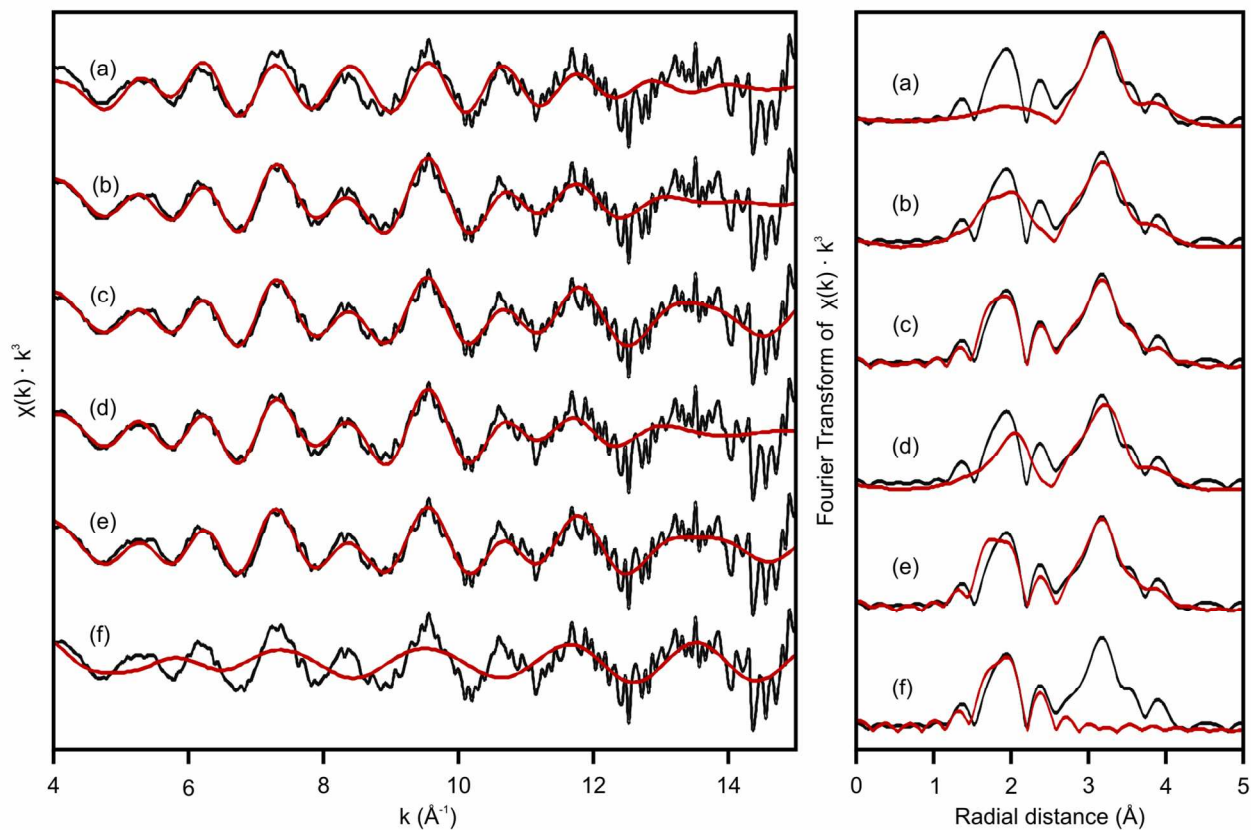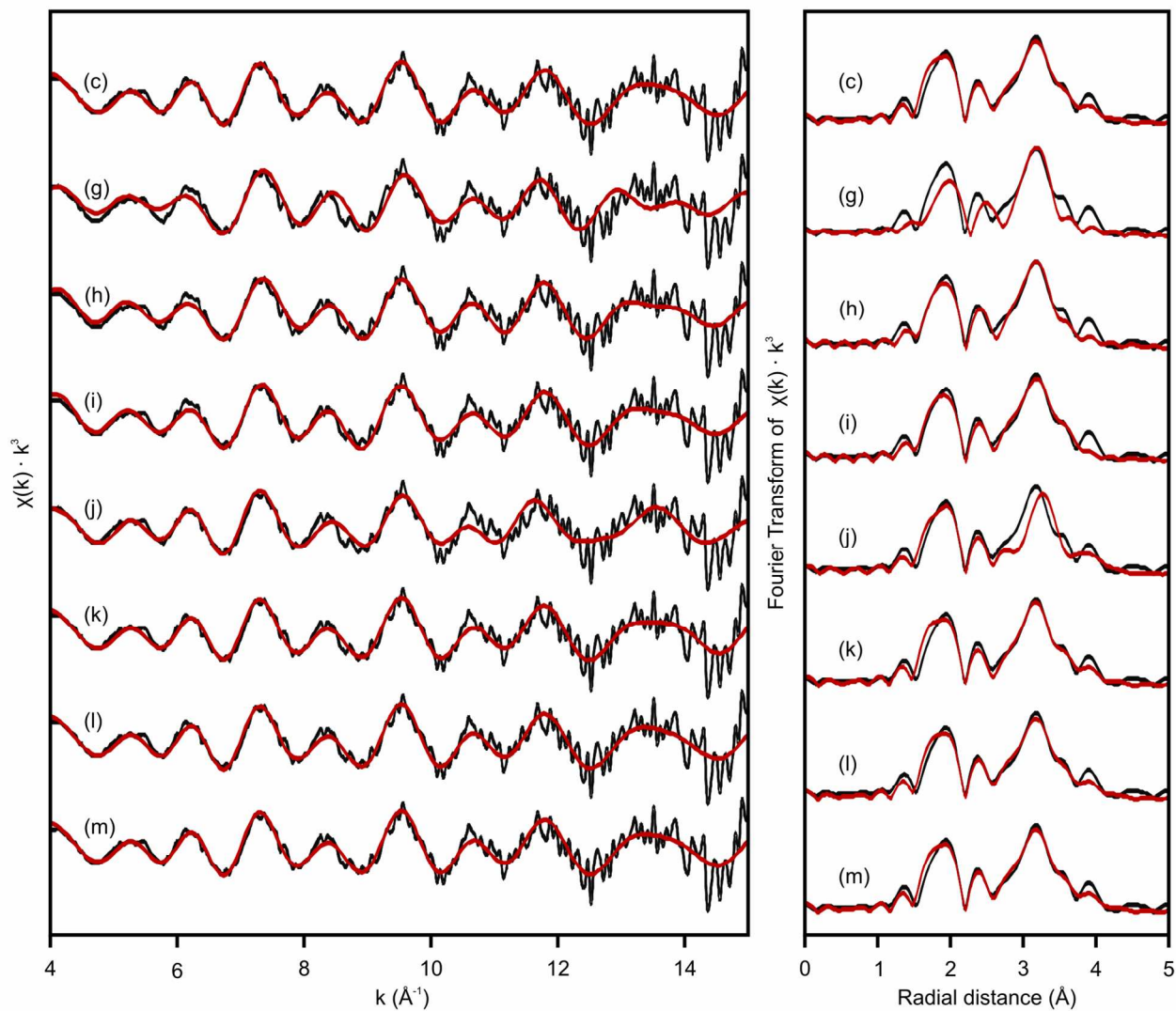
4 Table SI- 5.

5

6 Table SI- 3 Coordination numbers for Fe/O shells within the fitting models applied to the 105°C data.

Fit	(c)	(g)	(h)	(i)	(j)	(k)	(l)	(m)
O_{ax}	2	2	2	2	2	2	2	2
O_{eq1}	2	2	2	2	2	2	2	2
O_{eq2}	2	2	2	2	2	2	2	2
Fe_F	1	1	1	1		1	1	1
Fe_E	3		3	3	3	2	3	3
Fe_{C2}	3			3	3	3	2	3
Fe_{C2}	6				6	6	6	5
$O_{ax\ MS}$*	2	2	2	2	2	2	2	2

7   Blank cell indicates shell was omitted from the fitting model

8

Figure SI- 4 EXAFS fits (red) to 105°C data (black). Details of fit and fit parameters are given in Table SI- 5. The Fourier Transforms are plotted with a phase correction calculated from O_{ax} in each case.

1   **EXAFS Fitting – 60 °C data; effect of additional Fe shells and uncoordinated Fe shells**

2   The results of iterative fits to the 60°C data are presented below. The coordination number of the

3   shells is shown in Table SI- 4 and the fit plots are shown in Figure SI- 5. Details of the fit parameters are

4   given in Table SI- 5.

5

6   Table SI- 4 Coordination numbers for Fe/O shells within the fitting models applied to the 60°C data.

Fit	(n)	(o)	(p)	(q)	(r)	(s)
O_{ax}	2	2	2	2	2	2
O_{eq1}	2	2	2	2	2	2
O_{eq2}	2	2	2	2	2	2
Fe_F	1	1	1			1
Fe_E		3	3	3	3	2
Fe_{C2}			3		3	
Fe_{C2}						
$O_{ax\ MS}{}^{*}$	2	2	2	2	2	2

7   Blank cell indicates shell was omitted from the fitting model

8
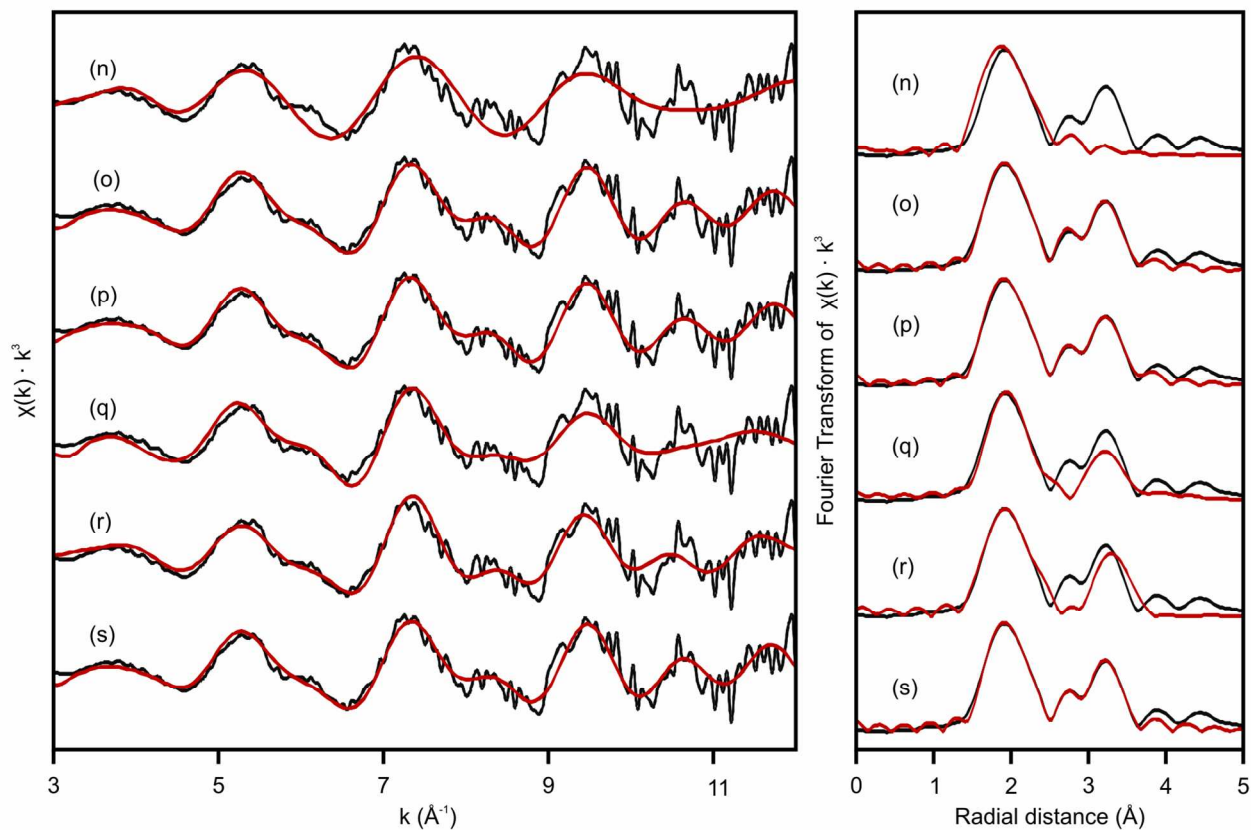
Figure SI- 5 EXAFS fits (red) to 60°C data (black). Details of fit and fit parameters are given in Table SI- 5. The Fourier Transforms are plotted with a phase correction calculated from O_{ax} in each case.

1   Table SI- 5 Parameters for fits (a) to (k)

Fit	Path	CN	R (Å)	σ^2 (Å^2)	ΔE_0 (eV)	$S0^2$	χ_v^2	R
(a)	O_{eq}	6	2.12 (11)	0.032 (7)	-10.0 ± 19.1	1.05 (1)	141.5	0.257
	Fe_F	1	2.89 (7)	0.011 (8)				
	Fe_E	3	3.12 (5)	0.010 (3)				
	Fe_{C1}	3	3.40 (11)	0.012 (9)				
	Fe_{C2}	6	3.97 (23)	0.02 (7)				
(b)	O_{ax}	2	1.83 (4)	0.008 (4)	-10.0 ± 11.5	0.85 (72)	57.6	0.088
	O_{eq}	4	2.10 (5)	0.012 (6)				
	Fe_F	1	2.85 (4)	0.009 (5)				
	Fe_E	3	3.10 (3)	0.011 (3)				
	Fe_{C1}	3	3.42 (10)	0.012 (7)				
	Fe_{C2}	6	3.96 (14)	0.021 (10)				
	$O_{ax\ MS}{}^{*}$	2	3.67 (7)	0.017 (8)				
(c)	O_{ax}	2	1.87 (2)	0.007 (2)	-4.4 ± 6.0	0.85 (6)	27.5	0.018
	O_{eq1}	2	2.07 (2)	0.003 (1)				
	O_{eq2}	2	2.23 (3)	0.005 (2)				
	Fe_F	1	2.87 (3)	0.007 (2)				
	Fe_E	3	3.11 (2)	0.010 (2)				
	Fe_{C1}	3	3.45 (6)	0.016 (7)				
	Fe_{C2}	6	4.01 (6)	0.024 (7)				
	$O_{ax\ MS}{}^{*}$	2	3.74 (4)	0.014 (3)				
(d)	O_{ax}	2	1.86 (4)	0.013 (5)	-10.0 ± 1.4	0.95 (75)	85.2	0.125
	O_{eq}	2	2.11 (2)	0.007 (5)				
	Fe_F	1	2.84 (5)	0.010 (5)				
	Fe_E	3	3.11 (3)	0.012 (4)				
	Fe_{C1}	3	3.42 (3)	0.012 (8)				
	Fe_{C2}	6	3.97 (4)	0.022 (12)				
	$O_{ax\ MS}{}^{*}$	2	3.72 (8)	0.026 (11)				

Fit	Path	CN	R (Å)	σ^2 (Å^2)	ΔE_0 (eV)	$S0^2$	χ_v^2	R
(e)	O_{ax}	2	1.85 (3)	0.005 (2)	-8.1 ± 10.1	0.85 (11)	45.8	0.030
	O_{eq1}	3	2.05 (4)	0.006 (2)				
	O_{eq2}	3	2.22 (6)	0.009 (3)				
	Fe_F	1	2.87 (4)	0.008 (3)				
	Fe_E	3	3.11 (3)	0.009 (2)				
	Fe_{C1}	3	3.42 (7)	0.014 (9)				
	Fe_{C2}	6	3.97 (11)	0.021 (7)				
	$O_{ax\ MS}$*	2	3.69 (6)	0.011 (4)				
(f)	O_{ax}	2	1.87 (9)	0.007 (9)	-10.0 ± 28.3	0.85 (17)	711.3	0.066
	O_{eq1}	2	2.06 (10)	0.003 (5)				
	O_{eq2}	2	2.21 (16)	0.006 (10)				
	$O_{ax\ MS}$*	2	3.73 (17)	0.014 (17)				
(g)	O_{ax}	2	1.90 (3)	0.014 (3)	9.2 ± 3.4	1.05 (1)	82.3	0.185
	O_{eq1}	2	2.14 (2)	0.006 (2)				
	O_{eq2}	2	2.32 (3)	0.008 (3)				
	Fe_F	1	3.18 (2)	0.004 (1)				
	$O_{ax\ MS}$*	2	3.80 (5)	0.027 (6)				
(h)	O_{ax}	2	1.88 (2)	0.009 (1)	6.1 ± 2.1	0.89 (23)	35.2	0.058
	O_{eq1}	2	2.10 (2)	0.004 (2)				
	O_{eq2}	2	2.27 (2)	0.005 (2)				
	Fe_F	1	2.91 (2)	0.007 (2)				
	Fe_E	3	3.15 (2)	0.009 (2)				
	$O_{ax\ MS}$*	2	3.76 (3)	0.018 (3)				
(i)	O_{ax}	2	1.87 (2)	0.008 (2)	2.4 ± 3.1	0.85 (6)	31.4	0.037
	O_{eq1}	2	2.09 (2)	0.003 (1)				
	O_{eq2}	2	2.25 (2)	0.005 (2)				
	Fe_F	1	2.89 (3)	0.007 (2)				
	Fe_E	3	3.14 (2)	0.010 (1)				
	Fe_{C1}	3	3.54 (5)	0.021 (8)				
	$O_{ax\ MS}$*	2	3.75 (3)	0.016 (3)				

Fit	Path	CN	R (Å)	σ^2 (Å^2)	ΔE_0 (eV)	$S0^2$	χ_v^2	R
(j)	O_{ax}	2	1.86 (4)	0.008 (3)	-10.0 ± 7.9	0.85 (7)	80.3	0.103
	O_{eq1}	2	2.06 (3)	0.003 (2)				
	O_{eq2}	2	2.22 (5)	0.006 (4)				
	Fe_E	3	3.14 (3)	0.016 (4)				
	Fe_{C1}	3	3.43 (5)	0.009 (2)				
	Fe_{C2}	6	3.97 (11)	0.020 (5)				
	$O_{ax\ MS}$*	2	3.73 (7)	0.015 (6)				
(k)	O_{ax}	2	1.87 (2)	0.007 (2)	-6.4 ± 6.9	0.85 (14)	29.9	0.019
	O_{eq1}	2	2.06 (3)	0.003 (1)				
	O_{eq2}	2	2.22 (4)	0.005 (2)				
	Fe_F	1	2.89 (3)	0.009 (3)				
	Fe_E	2	3.11 (2)	0.007 (1)				
	Fe_{C1}	3	3.45 (8)	0.015 (7)				
	Fe_{C2}	6	3.99 (7)	0.023 (7)				
	$O_{ax\ MS}$*	2	3.73 (4)	0.014 (4)				
(l)	O_{ax}	2	1.87 (2)	0.007 (2)	-3.2 ± 5.0	0.85 (13)	28.6	0.019
	O_{eq1}	2	2.07 (2)	0.003 (1)				
	O_{eq2}	2	2.23 (3)	0.005 (2)				
	Fe_F	1	2.87 (3)	0.007 (2)				
	Fe_E	3	3.11 (2)	0.010 (2)				
	Fe_{C1}	2	3.47 (6)	0.014 (7)				
	Fe_{C2}	6	4.02 (6)	0.024 (6)				
	$O_{ax\ MS}$*	2	3.74 (4)	0.015 (4)				
(m)	O_{ax}	2	1.87 (2)	0.007 (2)	-4.0 ± 5.7	0.85 (10)	27.3	0.017
	O_{eq1}	2	2.07 (2)	0.003 (1)				
	O_{eq2}	2	2.23 (3)	0.005 (2)				
	Fe_F	1	2.87 (3)	0.007 (2)				
	Fe_E	3	3.11 (2)	0.010 (2)				
	Fe_{C1}	3	3.46 (6)	0.016 (7)				
	Fe_{C2}	5	4.01 (6)	0.022 (6)				
	$O_{ax\ MS}$*	2	3.74 (4)	0.015 (4)				

Fit	Path	CN	R (Å)	σ^2 (Å^2)	ΔE_0 (eV)	$S0^2$	χ_v^2	R
(n)	O_{ax}	2	1.80 (6)	0.006 (4)	-10.0 ± 12.0	0.85 (10)	230.8	0.193
	O_{eq1}	2	2.06 (9)	0.003 (6)				
	O_{eq2}	2	2.21 (9)	0.002 (5)				
	Fe_F	1	2.81 (18)	0.019 (18)				
	$O_{ax\ MS}$*	2	3.60 (12)	0.012 (9)				
(o)	O_{ax}	2	1.84 (1)	0.009 (1)	6.5 ± 2.9	0.85 (3)	30.7	0.013
	O_{eq1}	2	2.17 (4)	0.008 (4)				
	O_{eq2}	2	2.31 (6)	0.012 (9)				
	Fe_F	1	2.91 (2)	0.006 (2)				
	Fe_E	3	3.16 (2)	0.011 (1)				
	$O_{ax\ MS}$*	2	3.68 (3)	0.017 (3)				
(p)	O_{ax}	2	1.83 (2)	0.008 (2)	2.8 ± 5.8	0.85 (8)	62.9	0.012
	O_{eq1}	2	2.14 (5)	0.007 (6)				
	O_{eq2}	2	2.28 (5)	0.008 (9)				
	Fe_F	1	2.89 (4)	0.006 (2)				
	Fe_E	3	3.14 (3)	0.011 (2)				
	Fe_{C1}	3	3.53 (14)	0.029 (25)				
	$O_{ax\ MS}$*	2	3.66 (4)	0.017 (4)				
(q)	O_{ax}	2	1.85 (2)	0.009 (3)	10.0 ± 0.01	0.85 (3)	143.0	0.114
	O_{eq1}	2	2.18 (4)	0.008 (7)				
	O_{eq2}	2	2.34 (5)	0.011 (12)				
	Fe_E	3	3.20 (3)	0.015 (4)				
	$O_{ax\ MS}$*	2	3.70 (4)	0.018 (5)				
(r)	O_{ax}	2	1.82 (3)	0.008 (5)	-10.0 ± 3.1	0.85 (69)	128.3	0.069
	O_{eq1}	2	2.08 (3)	0.003 (8)				
	O_{eq2}	2	2.22 (3)	0.002 (9)				
	Fe_E	3	3.20 (7)	0.019 (8)				
	Fe_{C1}	3	3.45 (3)	0.009 (6)				
	$O_{ax\ MS}$*	2	3.64 (6)	0.015 (10)				

Fit	Path	CN	R (Å)	σ^2 (Å^2)	ΔE_0 (eV)	S0^2	χ_v^2	R
(s)	O$_{ax}$	2	1.84 (1)	0.009 (2)	5.6 ± 2.9	0.85 (12)	31.5	0.013
	O$_{eq1}$	2	2.16 (3)	0.007 (4)				
	O$_{eq2}$	2	2.31 (4)	0.010 (7)				
	Fe$_F$	1	2.92 (2)	0.007 (2)				
	Fe$_E$	2	3.16 (2)	0.007 (1)				
	O$_{ax\ MS}$*	2	3.68 (3)	0.017 (3)				

1   CN denotes coordination number; R denotes atomic distance; σ^2 denotes Debye-Waller factor; ΔE_0
2   denotes the shift in energy from the calculated Fermi level; S0^2 denotes the amplitude factor which was
3   constrained to between 0.85 and 1.05; X_v^2 denotes the reduced Chi square value; R denotes the
4   'goodness of fit' factor; $_{MS}$ denotes multiple scattering paths in the axial O-U-O unit. * the multiple
5   scattering paths considered were linear paths and their ΔR and σ^2 parameters were evaluated as
6   multiples of the corresponding single scattering path parameter. Numbers in parentheses are errors on
7   the last significant figure(s).

8

F-Test analysis of EXAFS fits

Following the methods of Downward et al.[9] we have performed a series of F-tests to determine if two fits are statistically significantly different, as a way of assessing if a change to the model has improved the fit (e.g. addition of a shell). The data used in the F-teet calculations are presented in Table SI- 6 and the results of the various F-tests preformed are presented in Table SI- 7. The parameter α is the statistical significance level that the null hypothesis can be rejected, i.e. a large α means that the two fits are indeed significantly different.

Table SI- 6 EXAFS fit data used in F-test calculations for fits (a) to (s)

Fit	(a)	(b)	(c)	(d)	(e)	(f)	(g)	(h)	(i)	(j)
T	105 °C	105 °C	105 °C	105 °C	105 °C	105 °C	105 °C	105 °C	105 °C	105 °C
df	6.3	4.3	2.3	4.3	2.3	0.0	8.3	6.3	4.3	4.3
χ^2	886.7	245.8	62.4	363.5	103.8	71.1	680.0	220.6	133.8	342.7
χ_v^2	141.5	57.6	27.5	85.2	45.8	711.3	82.3	35.2	31.4	80.3
R	0.257	0.088	0.018	0.125	0.030	0.066	0.185	0.058	0.037	0.103
$\sqrt{R}$	0.507	0.297	0.134	0.354	0.174	0.257	0.430	0.241	0.192	0.321

Fit	(k)	(l)	(m)	(n)	(o)	(p)	(q)	(r)	(s)
T	105 °C	105 °C	105 °C	60 °C	60 °C	60 °C	60 °C	60 °C	60 °C
df	2.3	2.3	2.3	5.6	3.6	1.6	5.6	3.6	3.6
χ^2	66.4	64.8	62.0	1282.7	109.4	97.9	794.7	456.5	112.0
χ_v^2	29.3	28.6	27.3	230.8	30.7	62.9	143.0	128.3	31.5
R	0.019	0.019	0.018	0.193	0.013	0.012	0.114	0.069	0.013
$\sqrt{R}$	0.136	0.137	0.133	0.439	0.115	0.108	0.338	0.262	0.114

T denotes experimental temperature; df denotes the degrees of freedom; X^2 denotes the chi square value; X_v^2 denotes the reduced chi square value; R denotes the 'goodness of fit' factor; $\sqrt{R}$ denotes the square-root of R.

1   Table SI- 7 F-test results

F Test	α (%)	Comment
105 °C data		
(a) vs (b)	96.5	Addition of U-O_{ax} significantly improves fit
(b) vs (c)	96.7	Splitting the U-O_{eq} shell into two significantly improves fit
(c) vs (d)	98.4	Changing total U-O coordination from 6 to 4 significantly worsens fit
(c) vs (e)	31.9	Changing total U-O coordination from 6 to 8 worsens fit
(c) vs (f)	98.8	Excluding the Fe shells significantly worsens fit
(g) vs (h)	99.2	Addition of Fe_E significantly improves fit
(h) vs (i)	76.3	Addition of Fe_{C1} greatly improves fit
(i) vs (c)	78.7	Addition of Fe_{C2} greatly improves fit
(c) vs (j)	97.6	Omission of Fe_F significantly worsens fit
(c) vs (k)	0.0	Under co-ordination of Fe_E as charge compensation does not change the fit
(c) vs (l)	0.0	Under co-ordination of Fe_{C1} as charge compensation does not change the fit
(c) vs (m)	0.0	Under co-ordination of Fe_{C2} as charge compensation does not change the fit
60 °C data		
(n) vs (o)	99.9	Addition of Fe_E significantly improves fit
(o) vs (p)	22.2	Addition of Fe_{C1} does not change the fit
(o) vs (q)	99.7	Omission of Fe_F significantly worsens fit
(o) vs (r)	99.9	Omission of Fe_F but addition of Fe_{C1} significantly worsens the fit
(o) vs (s)	0.0	Under co-ordination of Fe_E as charge compensation does not change the fit

2

3

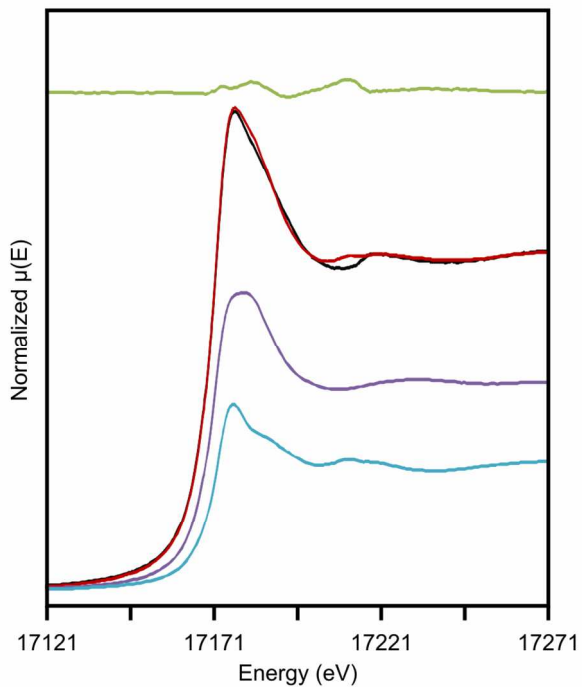1 **Linear combination fitting of 60°C data**

2 Linear combination fitting was performed in Athena[10] on two sets of EXAFS data collected at

3 different time points from the 60°C hematite ageing experiment; after 24 hours and after 30 days. Two

4 end member standards were used, these being the 0 hour (adsorbed) and 105°C 45 day (incorporated)

5 datasets. The fits were performed in both normalized $\mu(E)$ space and k space, with both standards

6 required in each fit. The weights of the standards were forced to between 0 and 1 and also to sum to 1.

7 The fit results from the two fitting spaces for each sample are within error, providing confidence in the

8 results. The relative proportions of the two end-members are similar to the results of the chemical

9 extractions (24hours = 48 % incorporated; 30 days = 69 % incorporated) but the chemical extractions

10 underestimate the incorporated U pool by approximately 10% versus the linear combination fits. The

11 results of the linear combination fitting are given in Table SI- 8 and plotted in Figure SI- 6 to Figure SI-

12 9.

13

14 Table SI- 8 Linear Combination fitting results for 24 hours and 30 days samples aged at 60°C

Sample	24 hours				30 days			
Fitting space	normalized $\mu(E)$		$\chi(k)$		normalized $\mu(E)$		$\chi(k)$	
Fit range	-50 to 100 eV		3.0 – 12.0		-50 to 100 eV		3.0 – 12.0	
R	0.00056		0.25		0.00017		0.26	
χ^2	0.0179		82.5		0.0117		48.8	
χ_v^2	0.00012		0.46		0.000038		0.27	
Standard	0 hour	105°C	0 hour	105°C	0 hour	105°C	0 hour	105°C
weight (%)	38 ± 2	62 ± 2	41 ± 2	59 ± 2	20 ± 1	80 ± 1	24 ± 2	76 ± 2
E_0	0.1 ± 0.2	-0.3 ± 0.1	0.1 ± 0.2	-0.3 ± 0.1	-0.3 ± 0.2	0.0 ± 0.0	0.1 ± 0.2	-0.3 ± 0.1

15 In a given fit: both standards were required in the fit; all weights were forced to between 0 and 1; all
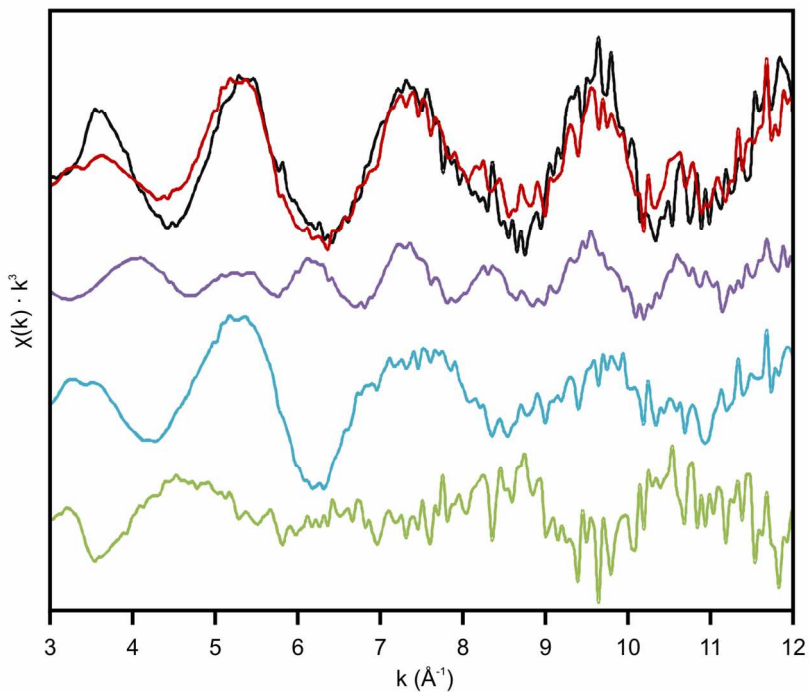16 weights were forced to sum to 1.

17

1

2 Figure SI- 6 Linear combination fit to 24 hour data in E space. Black line is the data. Red line is the fit
3 to the data. Green line is the residual. Purple line is the scaled contribution from the 105°C 'standard'.
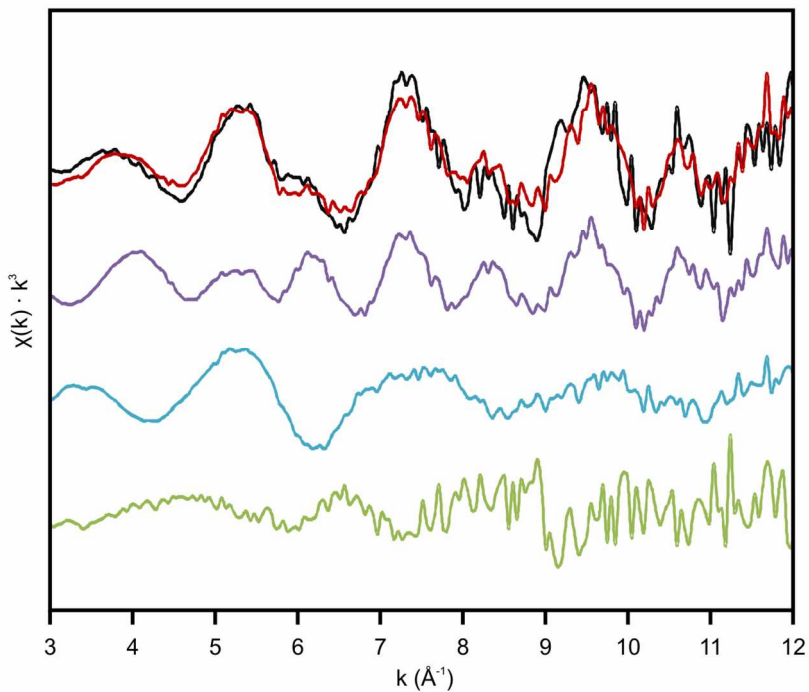4 Blue line is the scaled contribution from the 0 hour 'standard'.
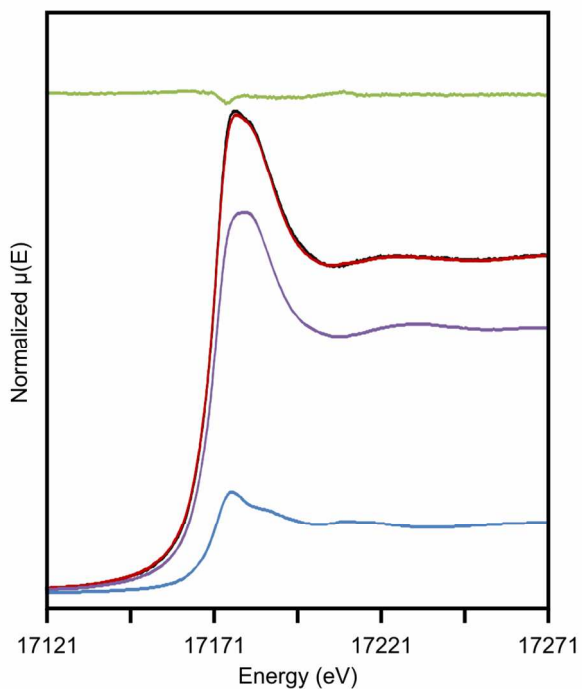
5

6 Figure SI- 7 Linear combination fit to 30 day data in E space. Black line is the data. Red line is the fit to
7 the data. Green line is the residual. Purple line is the scaled contribution from the 105°C 'standard'. Blue
8 line is the scaled contribution from the 0 hour 'standard'.

Figure SI- 8 Linear combination fit to 24 hour data in k space. Black line is the data. Red line is the fit to the data. Green line is the residual. Purple line is the scaled contribution from the 105°C 'standard'. Blue line is the scaled contribution from the 0 hour 'standard'.

Figure SI- 9 Linear combination fit to 30 day data in k space. Black line is the data. Red line is the fit to the data. Green line is the residual. Purple line is the scaled contribution from the 105°C 'standard'. Blue line is the scaled contribution from the 0 hour 'standard'.

REFERENCES

(1)   Cornell, R. M.; Schwertmann, U. *The Iron Oxides: Structure, Properties, Reactions, Occurences and Uses*; 2nd Editio.; Wiley-VCH: Weinham, 2003.

(2)   Viollier, E.; Inglett, P. W.; Hunter, K.; Roychoudhury, A. N.; Van Cappellen, P. The Ferrozine Method Revisited: Fe(II)/Fe(III) Determination in Natural Waters. *Appl. Geochemistry* **2000**, *15*, 785–790.

(3)   Nuclear Decommissioning Authority. *Geological Disposal: Near-Field Evolution Status Report*; 2011.

(4)   Bruker AXS. Topas V4-2: General Profile and Structure Analysis Software for Powder Diffraction Data. User's Manual, 2009.

(5)   Rietveld, H. M. A Profile Refinement Method for Nuclear and Magnetic Structures. *J. Appl. Crystallogr.* **1969**, *2*, 65–71.

(6)   Hill, R. J.; Howard, C. J. Quantitative Phase-Analysis from Neutron Powder Diffraction Data Using the Rietveld Method. *J. Appl. Crystallogr.* **1987**, *20*, 467–474.

(7)   Michel, F. M.; Ehm, L.; Antao, S. M.; Lee, P. L.; Chupas, P. J.; Liu, G.; Strongin, D. R.; Schoonen, M. a a; Phillips, B. L.; Parise, J. B. The Structure of Ferrihydrite, a Nanocrystalline Material. *Science* **2007**, *316*, 1726–9.

(8)   Zabinsky, S. I.; Rehr, J. J.; Ankudinov, A.; Albers, R. C.; Eller, M. J. Multiple-Scattering Calculations of X-Ray-Absorption Spectra. *Phys. Chem. Chem. Phys.* **1995**, *52*, 2995–3009.

(9)   Downward, L.; Booth, C. H.; Lukens, W. W.; Bridges, F. A Variation of the F-Test for Determining Statistical Relevance of Particular Parameters in EXAFS Fits. In *X-Ray Absorption Fine Structure-XAFS13*; Hedman, B.; Painetta, P., Eds.; 2007; Vol. 882, pp. 129–131.

(10) Ravel, B.; Newville, M. ATHENA, ARTEMIS, HEPHAESTUS: Data Analysis for X-Ray Absorption Spectroscopy Using IFEFFIT. *J. Synchrotron Radiat.* **2005**, *12*, 537–541.